Numerical Simulation of Droplet Generation Mode Transition of Co-flowing Liquids in Micro-channel

Jinsong Hua [1], Ming Cheng [2] and Tiegang Liu [3]

Institute of High Performance Computing
1 Science Park Road, #01-01 The Capricorn, Singapore Science Park II, Singapore 117528
[1] huajs@ihpc.a-star.edu.sg; [2] chengm@ihpc.a-star.edu.sg; [3] liutg@ihpc.a-star.edu.sg

ABSTRACT

Droplet formation in a co-flowing liquid system is simulated using the front tracking method to investigate the mechanism of droplet generation under the dripping and jetting modes, and the mode transition, which is critical in the design of micro-fluidic devices to produce mono-disperse droplets. The Navier-Stokes equations for the two liquid phases are solved numerically on a fixed Eulerian cylindrical coordinate mesh for the fluid flows, and the front tracking method is applied to track the movement of the interface between the two immiscible liquids as well as the calculation of surface tension. The simulations reasonably predict the droplet formation modes in the co-flowing liquids and the detailed flow dynamics. Under certain critical scenarios, a slight change of the flow condition, e.g. outer liquid flow velocity, may cause abrupt mode transition, resulting in great change in the size of droplet produced. It is also found that the formation of a dispersed liquid cone-jet is the key phenomenon that relates to the droplet generation modes. The mode transition is caused upon the balance of the fluid flow inertia and the capillary pressure in the dispersed liquid cone-jet.

Keywords: numerical simulation, front tracking method, micro-fluidics, droplet generation, mono-dispersed droplet.

1 INTRODUCTION

With the merging of new technologies of BioMEMS and Lab-On-Chip, droplets / emulsions can provide ideal microcapsules that can isolate reactive materials, cells or drugs and transport them in micro-channels. A fairly simple yet common way of producing a dispersion of droplets is by injecting the dispersed liquid from a capillary tube into a bath of a second immiscible liquid co-flowing in an outer micro-channel as shown in Figure 1. Experimental studies have discovered that there are two modes of droplet formation, i.e. dripping and jetting, depending upon liquid flow rate, viscosity, interface tension, etc. Cramer et al [1] and Utada et al [2] revealed that the droplet sizes formed in these two modes are quite different, and that the mode transition could occur abruptly by varying the outer liquid flow rate slightly under certain critical flow condition. Hence, to generate mono-dispersed droplets in such microfluidic devices, it is importance to understand the mechanism of droplet generation and the conditions under which the mode transition occurs.

Ganan-Calvo and Riesco-Chueca [3] studied the jetting-dripping transition of viscous jet under the influence of a viscous flowing ambient. They presented a theoretical analysis considering the spatio-temporal stability of a core liquid jet produced by flow focusing. Sevilla et al [4] investigated experimentally the transition from bubbling to jetting in co-axial air-water jet, and proposed a simple explanation for the transition based on linear, local, spatio-temporal stability theory. Suryo and Basaran [5] investigated the formation of tip streaming from a liquid drop produced from a tube in a co-flowing outer liquid by numerical simulation. They solved the governing Stokes equations.

In this study, a front tracking method based multiphase flow simulation [6, 7] is adopted to simulate the transition dynamics of droplet formation of the co-flowing liquids in a micro-channel. Here, one set of Navier-Stokes equations for the two liquid phases is solved on a fixed Eulerian two-dimensional cylindrical coordinate mesh for the fluid flow dynamics. The front tracking method is applied to track the movement of the interface between the two immiscible liquids, and accounts for the surface tension. It provides a first principle approach for the numerical simulation of droplet formation dynamics.

2 MATHEMATICAL FORMULATION AND NUMERICAL METHOD

2.1 Physical Problem

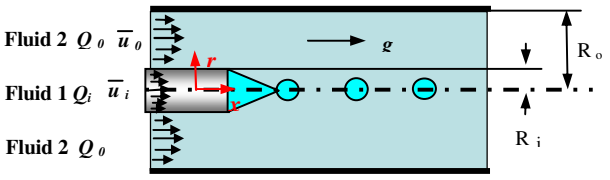

Figure 1: Schematic diagram of droplet formation from a capillary nozzle in a co-flowing viscous liquid.

A typical co-flowing system of two viscous immiscible liquids is illustrated in Figure 1. The dispersed liquid (Fluid 1) is injected into the system through a capillary nozzle with a radius of R_i into the co-flowing liquid (Fluid

NSTI-Nanotech 2007, www.nsti.org, ISBN 1420061844 Vol. 3, 2007

2) in a coaxial cylindrical tube with an inner radius of R_o. Both the dispersed phase and the continuous phase are injected into the system continuously at constant flow rates of Q_i and Q_o, respectively. As the two fluid phases are immiscible, an axis-symmetric interface is formed between two liquid streams. The interface evolves and collapses to form droplets while the two immiscible liquid phases are flowing through the system.

2.2 Governing Equations and Boundary Conditions

The fluid properties such as density and viscosity for both phases are assumed to be constant while they flow through the system. Hence, it is reasonable to treat the liquid phase incompressible, and the mass conservation equation in the whole domain can be expressed as,

$$\nabla \cdot \mathbf{u} = 0 . \tag{1}$$

The Navier-Stokes equation, governing the momentum balance in each fluid phase and on the interface, can be expressed as,

$$\frac{\partial(\rho \mathbf{u})}{\partial t} + \nabla \cdot \rho \mathbf{u}\mathbf{u} = -\nabla p + \nabla \cdot [\mu(\nabla \mathbf{u} + \nabla^T \mathbf{u})] + \sigma \kappa \mathbf{n}\, \delta(\mathbf{x} - \mathbf{x}_f) + (\rho_o - \rho)\mathbf{g} \tag{2}$$

where $\delta(\mathbf{x} - \mathbf{x}_f)$ is a delta function that is zero everywhere except at the interface, $\mathbf{g}$ is the gravitational acceleration, and subscript f refers the interface. ρ is the density of fluids, and ρ_o is the density of the continuous liquid phase.

For the initial conditions, a flat interface at the tip of the inner capillary tube and a stationary flow for the entire domain are assumed. And the following conditions are applied to the boundaries. At the upstream of the inner capillary tube, a fully developed laminar flow velocity profile is set,

$$u_i(r) = 2\,\bar{u}_i \left[1 - \left(\frac{r}{R_i} \right)^2 \right] \qquad \text{for} \quad 0 \le r \le R_i , \tag{3}$$

Similarly, the velocity profile of fully developed laminar flow of the outer continuous phase flowing in the annulus is imposed,

$$u_o(r) = 2\,\bar{u}_o \times \frac{\left[1 - \left(\frac{r}{R_o} \right)^2 + \frac{1 - (R_i / R_o)^2}{ln(R_o / R_i)} ln(r / R_o) \right]}{\left(1 + \frac{R_i}{R_o} - \frac{1 - (R_i / R_0)^2}{ln(R_o / R_i)} \right)} \tag{4}$$

$$\text{for } R_i \le r \le R_o ,$$

where $\bar{u}_i$ and $\bar{u}_o$ are the averaged flow speed of the disperse phase and continuous liquid phase, respectively.

On all the walls, a non-slip boundary condition is applied. A symmetric boundary condition is applied along the central axis. An outflow boundary condition is applied at the right most boundary of the solution domain.

In addition, we introduce the following dimensionless characteristic variables,

$$x^* = \frac{x}{R_i};\quad u^* = \frac{u}{(gR_i)^{1/2}};\quad \tau = \frac{t}{R_i^{1/2} g^{-1/2}};\quad \rho^* = \frac{\rho}{\rho_i};$$

$$p^* = \frac{p}{\rho_i g R_i};\quad \mu^* = \frac{\mu}{\mu_i};\quad \kappa^* = \frac{\kappa}{R_i^{-1}}$$

where the radius of the capillary nozzle, R_i, is used as characteristic length, and the gravity based characteristic velocity $(gR_i)^{1/2}$ is used as characteristic velocity. Hence, the non-dimensional Navier-Stokes equation could be re-expressed as,

$$\frac{\partial(\rho \mathbf{u})}{\partial t} + \nabla \cdot \rho \mathbf{u}\mathbf{u} = -\nabla p + \frac{1}{\mathrm{Re}} \nabla \cdot [\mu(\nabla \mathbf{u} + \nabla^T \mathbf{u})] + \frac{1}{\mathrm{Bo}} \kappa \mathbf{n}\, \delta(\mathbf{x} - \mathbf{x}_f) + (\rho - 1) \tag{5}$$

in which the superscript * is omitted for convenience. The non-dimensional Reynolds number and Bond number are defined as follows,

$$\mathrm{Re} = \frac{\rho_i g^{1/2} R_i^{3/2}}{\mu_i};\quad Bo = \frac{\rho_i g R_i^{\,2}}{\sigma} . \tag{6}$$

Based on the above formulation, the problem of micro-droplet formation in a co-flowing liquid could be characterized by the following non-dimensional parameters, namely, the ratios of density (ρ_o / ρ_i) and viscosity (μ_0 / μ_i) of two fluids, Reynolds number (Re), Bond number Bo, velocity ratio ($\bar{u}_o / \bar{u}_i$) and geometry ratio (R_o / R_i).

2.3 Interface Treatment and Tracking

The material property fields over whole domain may be reconstructed using an indicator function $I(\mathbf{x}, t)$, which has the value of one in the one liquid phase and zero in another liquid phase at a given time t.

$$b(\mathbf{x}, t) = b_o + (b_i - b_o) I(\mathbf{x}, t) ; \tag{7}$$

$$I(\mathbf{x}, t) = \int_{\Omega(t)} \delta(\mathbf{x} - \mathbf{x}') d\mathbf{v}' \tag{8}$$

in which b stands for either fluid density or viscosity. The indicator function can be obtained in the form of an integral of $\delta(\mathbf{x} - \mathbf{x}')$ over the whole domain. The novelty of the front tacking method proposed by Tryggvason and co-workers [6] is that the front is considered to have a finite thickness of the order of the background mesh size instead of zero thickness. Hence, the delta function is approximated by the following distribution function,

$$D(\mathbf{x} - \mathbf{x}_f) = \begin{cases} (4h)^{-2} \prod_{i=1}^{2} \left(1 + \cos\left(\frac{\pi}{2h} |\mathbf{x} - \mathbf{x}_f| \right) \right), & \text{if } |\mathbf{x} - \mathbf{x}_f| < 2\mathrm{h} \\ 0, & \text{otherwise.} \end{cases} \tag{9}$$

where h is the grid size.

When the fluid velocity is updated on the fixed grid, the moving velocity of the element nodes on the interface could be interpolated from the background grid to ensure that the front moves at the same velocity as the surrounding fluids.

$$\mathbf{u}_f = \sum D(\mathbf{x}_f - \mathbf{x})\mathbf{u}(\mathbf{x}). \quad (10)$$

Then, the interface is advected in a Lagrangian fashion with time step size Δt ,

$$\mathbf{x}_f^{n+1} - \mathbf{x}_f^{n} = \Delta t \ \mathbf{u}_f \ . \quad (11)$$

In the present work, the interface front is marked by a set of connected line elements. There are 4-10 line elements within one background grid cell.

3 RESULTS AND DISCUSSION

3.1 Droplet Generation in Dripping and Jetting Modes

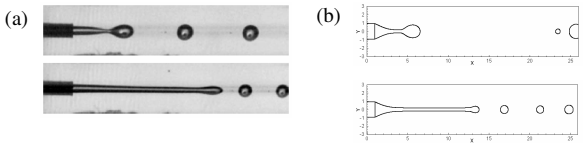

Figure 2: The typical dripping and jetting modes (a) observed in the experiments by Cramer et al [1] and (b) predicted in the simulation.

Cramer et al [1] studied the drop formation in a co-flowing ambient fluid. Their experimental results revealed that there were two modes of droplet formation, as shown in Figure 2(a), depending upon the flow speed ratio of the continuous phase to the disperse phase and the fluid properties such as viscosity. Numerical simulations are performed to investigate the droplet formation mechanism in the micro-channel with the similar set up. Quantitative comparison between the simulation and experiment is not made here due to the different scale of the problem. In the simulation, the dimension ratio of the channel size to the capillary needle diameters is much smaller comparing to that in the experiments [1]. However, the droplet formation modes, i.e. dripping and jetting, are well predicted in the simulation, which agrees with experimental observation as shown in Figure 2.

3.2 Effect of Continuous Phase Flow Speed on the Drop Generation

The effect of the continuous phase liquid flow speed on the size of the droplets formed in the micro-channel by co-flowing liquids is shown in Figure 3. All other parameters are set to constant values as $\mathrm{Re} = 0.1$; $Bo = 0.001$; $\rho^* = 0.8$; $\mu^* = 1.5$; $R_o / R_i = 3.0$ and $\overline{u}_i = 1.0$ except the outer flow velocity ($\overline{u}_o$). The simulation results indicate the droplet generation mode changes form dripping to jetting while increasing the flow velocity of the continuous phase. In each droplet generation mode, the droplet size varies smoothly with the continuous change of the outer liquid flow speed with power law correlations. However, the droplet size shows significant variation when the transition of the droplet generation mode occurs within a very small region of the outer liquid phase speed at certain critical condition. Similar phenomenon has been observed in a number of previous experimental works [1, 2]. The abrupt change of the droplet generation mode and droplet size formed over a small variation of outer flow speed may create huge challenges on the micro-fluidic device design/operation to produce mono-dispersed droplets. Hence, a detailed study on the droplet generation mode transition is presented in the following section.

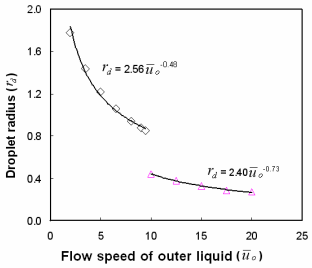

Figure 3: Effect of the flow speed of the continuous liquid phase on the droplet size.

3.3 Dynamics of the Droplet Formation in Dripping and Jetting Modes

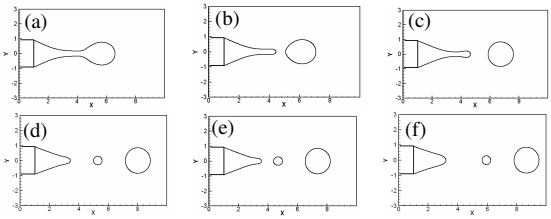

Figure 4: The initial stage of droplet evolution in the dripping mode when $\overline{u}_o = 9.5$.

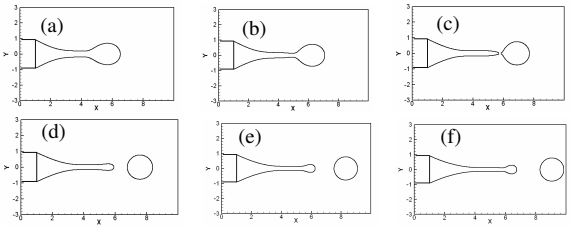

Figure 5: The initial stage of droplet evolution in the jetting mode when $\overline{u}_o = 11$.

To understand the dynamics of droplet formation and mode transition, we focus on the transient simulation of the liquid thread/jet breakup during the initial droplet generation process under the outer liquid flow speeds of $\overline{u}_o = 9.5$ and $\overline{u}_o = 11$ where the mode transition occurs. The

NSTI-Nanotech 2007, www.nsti.org, ISBN 1420061844 Vol. 3, 2007

simulation results are shown in Figures 4 and 5. The liquid thread of the dispersed liquid is dragged and stretched along by the shear viscous force from the continuous phase. When the speed of the dispersed liquid thread is fast enough, the liquid thread will start to narrow at the place where it has the highest velocity to conform with the principle of mass conservation. Due to the high surface tension force, a high capillary pressure is created at the tip of the liquid thread, and the dispersed liquid will be slowed down. Hence, the accumulated dispersed liquid at the liquid thread tip grows into a droplet as shown in Figures 4(a) and 5(a) & (b). Further narrowing of the liquid thread leads to its break up of liquid thread, and forms a separated droplet. The remaining part of the dispersed liquid thread attaches to the capillary nozzle and forms a cone shape with a fine jet as shown in Figures 4 (b) and 5(c). Then, the tip of the fine jet starts to recoil back due to surface tension as shown in Figures 4(c) and 5(d).

In the dripping mode, the fine jet will fully retract back, or lead to further break up to form satellite droplets as shown in Figures 4(d) and 4(e). Finally, a cone shaped dispersed liquid thread is remaining at the outlet of capillary nozzle as shown in Figure 4(f). Further growing of the liquid thread cone starts the next cycle of droplet formation. In the jetting mode, the fine jet cannot fully retract back due to the higher shear viscous force from the higher speed flow of the outer continuous liquid and high flow inertia of the dispersed phase at the upstream. The fine jet actually is further stretched and elongated as shown in Figures 5(e) and 5(f). Finally, the breakup of the fine jet into small droplet occurs due to the development of jet instability.

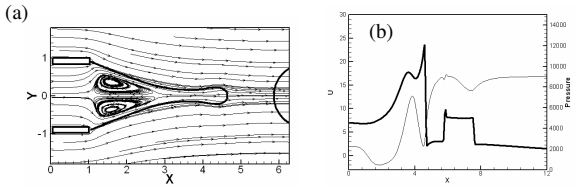

Figure 6: (a) The flow path in the cone-jet and (b) the distributions of pressure (thick line) and axial (thin line) velocity along central axis under the dripping mode.

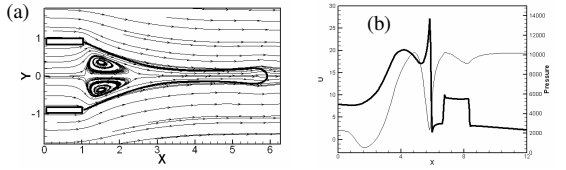

Figure 7: (a) The flow path in the cone-jet and (b) the distribution pressure (thick line) and velocity (thin line) along central axis under the jetting mode.

A detail comparison of the flow pattern and flow dynamic within the dispersed liquid cone-jet is shown in Figures 6 and 7 respectively for the cases shown in Figure 4(c) and Figure 5(d). The plots of flow path line shown in Figure 6(a) and 7(a) indicate that the flow circulation is formed in the dispersed liquid cone due to strong shear viscous force acting on the interface between the inner and outer viscous liquids. The pressure and flow velocity distributions along the central axis within the cone-jet are shown in Figure 6(b) and 7(a). The flow speed increases after the circulation zone as the liquid interface converges to form the jet. As the interface converges in the liquid cone to form a jet, the shrinkage of the radial dimension (high curvature) leads to high pressure in the jet that may slow down the upstream flow from the cone. Due to the similar shape of the liquid cone-jet and capillary force (surface tension force) on the interface, the pressure distributions along the central axis are quite similar under the two cases for dripping and jetting modes. However, velocity distributions along the central axis are different. It is obvious that a higher velocity peak can be reached in the jetting mode. Hence, under the jetting mode, the jet inertia finally overcomes the capillary pressure to stretch the jet further and avoid the recoiling of the jet. The breakup of the fine jet will produce finer droplets in the jetting mode.

4 CONCLUSION

Droplet formation in the co-flowing liquid has been simulated using a front tracking method. Two droplet generation modes are revealed. In the dripping mode the droplet is generated from the cone attached to the capillary nozzle, and in the jetting mode the droplet is generated from the tip of the fine jet generated from the base cone. The simulation results indicate that droplets are generated in dripping mode at a low outer liquid flow velocity, and in jetting mode at a high outer liquid velocity. The transition form dripping to jetting occurs abruptly when the outer liquid flow velocity is slight higher than a critical value. The detailed flow dynamics simulation of the droplet formation shows that the mode transition occurs when the jet inertia overcomes the capillary pressure. The development of jet inertia attributes to the exertion of shear viscous force from the outer flow, while the capillary pressure distribution in the jet mainly attributes to the surface tension and jet topology.

REFERENCES

[1] C. Cramer, P. Fischer and E. J. Windhab, Chem. Eng. Sci. **59,** 3045 (2004).

[2] S. Utada, E. Lorenceau, D. R. Link, P. D. Kaplan, H. A. Stone, and D. A. Weitz, Science **308,** 537 (2005).

[3] M. Ganan-Calvo and J. Riesco-Chueca, Fluid Mech. **553**, 75 (2006).

[4] Sevilla, J.M. Gordillo and C. Martinez-Bazan, Phys. Fluids **17**, 018105 (2005).

[5] R. Suryo and O.A. Basaran, Phys. Fluids **18**, 082102 (2006).

[6] S. O. Unverdi and G. Tryggvason, J. Comput. Phys. **100,** 25 (1992).

[7] J.S. Hua and J. Lou, J. Comput. Phys. **222**, 769 (2007).